Urol Res (2003) 31: 341–346
DOI 10.1007/s00240-003-0347-9

ORIGINAL PAPER

George A. Abrams · Christopher J. Murphy
Zun-Yi Wang · Paul F. Nealey · Dale E. Bjorling

Ultrastructural basement membrane topography of the bladder epithelium

Received: 3 December 2002 / Accepted: 4 July 2003 / Published online: 13 September 2003

Abstract The basement membrane underlies epithelium and separates it from deeper tissues. Recent studies suggest that nanoscale topography of the surface of basement membrane may modulate adhesion, migration, proliferation and differentiation of overlying epithelium. This study was performed to elucidate nanoscale topographic features of basement membrane of the bladder. Bladder tissues were obtained from three adult female rhesus macaques. A process was developed to remove the epithelium while preserving the underlying basement membrane, and tissues were evaluated by immunohistochemistry and scanning electron microscopy (SEM). Detailed measurements were made of stereo SEM images to quantitatively define topographic features. Measurements made from multiple SEM images of bladder basement membrane provided the following values for topographic features: mean feature height, 178 ± 57 nm; mean fiber diameters, 52 ± 28 nm; mean pore diameter, 82 ± 49 nm; and mean interpore distance (center to center), 127 ± 54 nm. These dimensions are similar to those reported previously for basement membranes of other species and anatomical locations. This information provides a rational basis for design of nanostructured biomaterials to produce composite grafts for repair or replacement of segments of the urinary tract.

Keywords Bladder · Basement membrane · Nanoscale topography

G. A. Abrams · C. J. Murphy · Z. Y. Wang · D. E. Bjorling (✉)
Department of Surgical Sciences,
School of Veterinary Medicine, University of Wisconsin-Madison,
2015 Linden Drive, Madison, WI 53711, USA
E-mail: bjorlind@svm.vetmed.wisc.edu
Tel.: +1-608-2634808
Fax: +1-608-2637930

P. F. Nealey
Department of Chemical Engineering,
College of Engineering, University of Wisconsin-Madison,
2015 Linden Drive, Madison, WI 53711, USA

Basement membranes are unique extracellular matrices that underlie a variety of epithelial cells and are generally composed of a complex mixture of constituents including collagen IV, laminin, entactin/nidogen, and sulfated proteoglycans [1, 2]. Cells attach themselves to the underlying stroma through the basement membrane, and it anatomically separates the epithelium from deeper tissues. It is clear from numerous studies that basement membranes modulate key cellular processes of the overlying epithelium, including adhesion, migration, proliferation and differentiation through biochemical interactions [3, 4, 5].

Synthesis of basement membrane by endothelial cells during capillary formation is essential to orderly assembly of blood vessels, and interference with this process disrupts formation of capillary tubes [6]. Proteins under the control of capillary morphogenesis genes are differentially regulated during formation of capillaries, and a subset of these proteins has a distinct affinity for the basement membrane [6]. The basement membrane may also serve to focus growth factors and their receptors as is the case for fibroblast growth factors and their cognate receptors during early epithelial morphogenesis in embryonic stem cell-derived embryoid bodies [7]. Signaling between the basement membrane and epithelium appears to occur in a reciprocal manner. Synthesis and assembly of the basement membrane is regulated to some degree by cytokines, particularly TGF-β1 [8], but excessive production of TGF-β1 by nascent epithelial cells results in defects within the basement membrane, and TGF-β1 may in part be responsible for damage to the basement membrane observed in conditions such as renal fibrosis [9, 10].

It has been observed that basement membranes have distinguishing topographical features, but prior studies have done little to quantify the characteristics of surface topography of the basement membrane at the nanoscale level [11, 12, 13]. Previous reports characterizing basement membranes indicate that a similar morphology exists from tissue to tissue, and it appears highly likely that basement membrane topography represents a

fundamental means by which the extracellular matrix modulates cellular functions [12, 13, 14, 15, 16, 17], because multiple investigators have reported that topographical features of the extracellular matrix (including the basement membrane) can influence cell behaviors [18].

The purpose of this investigation was to quantitatively define the nanoscale topography of the bladder basement membrane and to compare this to our previous observations of the basement membranes underlying the anterior and posterior corneal epithelium and of the basement membrane-like complex Matrigel® (Collaboration Research, Bedford, MA) [18, 19, 20].

Materials and methods

Bladder specimens were obtained from animals outside our laboratory that were euthanized in the course of other investigations and in accordance with the NIH guideline on the Care and Use of Animals in Research. Three bladders were obtained from female adult (7, 10, and 14 years old) rhesus macaques immediately after euthanasia. Initial experiments were performed using multiple bladder segments to optimize removal of the urothelium with minimal disturbance to the underlying basement membrane. Mechanical dissection of the mucosa from the underlying tissues was unsatisfactory due to the amount of damage to the basement membrane. Infusion of the bladders with EDTA followed by flushing with phosphate buffered saline (PBS) failed to adequately remove the epithelium. The technique that was found to be optimal was similar to that described by Spurr and Gibson [21]. Bladders were removed at the time of euthanasia, flushed with PBS, and placed in a beaker containing PBS for transport to the laboratory. Within 30 min, 1-cm^2 full-thickness sections of the body of the bladder were removed, stretched until increased in size by approximately 50%, and fixed to metal frames with suture material. Stretched tissues were incubated in 2.5 mM EDTA in Hepes buffer (Sigma, St. Louis, MO) at room temperature for 30 min, after which they were subjected to sonication (Crest Ultrasonic Cleaner, WI) in a beaker of PBS at 2 amps for 3 min. Specimens were then fixed (2% glutaraldehyde -Fisher, Pittsburg, PA; in 0.1 M pH 7.4 phosphate buffer for 12 at 8°C) and transferred to fresh phosphate buffer for preparation for scanning electron microscopy (SEM) or 4% paraformaldehyde for immunohistochemistry (IHC).

Immunohistochemistry

Immunohistochemistry was performed using antibodies to laminin and collagen IV to confirm that the basement membrane was still present after removal of the urothelium. Intact bladder specimens were also evaluated by IHC for comparison purposes. Samples of intact bladders and bladders from which the urothelium had been removed were fixed in 4% paraformaldehyde overnight at 4°C. Tissues were cryoprotected with 30% sucrose and frozen in embedding solution on dry ice. Sections (10 mm) were cut using a cryostat (Microm Laborgerate GmbH, Walldorf, Germany), then air-dried and rinsed in PBS several times. Slides were then treated with 10% normal goat serum for 2 h at room temperature in a humid chamber. Sections were incubated overnight at 4°C with each specific antibody. To reveal staining, sections were incubated with a FITC-conjugated goat anti-rabbit IgG (1:250; Sigma, St. Louis, MO) for 90 min at room temperature. Sections were rinsed, coverslipped using an anti-fading solution (Vectashield, Vector laboratories Inc., Burlingame, CA), and examined with a Nikon E600 microscope. Images were captured using a digital camera (Diagnostic Instruments, Sterling Heights, MI). For negative controls, tissue sections were incubated with normal rabbit IgG instead of specific antibodies. The following antibodies (rabbit origin) were used: laminin (anti-mouse; 1:200, Sigma-Aldrich, St. Louis, MO) and collagen IV (anti-human; 1:1000, Sigma-Aldrich, St. Louis, MO).

SEM

Bladders were prepared for SEM by dehydration through an ethanol series and critical point dried with CO_2 [22]. Samples were then ion-beam coated with 2–4 nm of platinum (Ion Tech, Teddington, England). Scanning electron microscopy was performed with a low-voltage, high-resolution scanning electron microscope (Hitachi S-900, Japan) at 1.5 keV. Stereo pair images were obtained at ± 5.0-degree tilt angles from the horizontal. For quantification of the matrix feature height, the parallax shift in stereo pairs was measured and the height was calculated using the formula $Z = (P/2\sin(\text{alpha}/2))$, where Z = height P = parallax shift, and alpha is the half angle of the stereo pair [22, 23]. A minimum of ten random height measurements were calculated from each stereo pair image. The fiber and pore diameters were measured at 30,000× magnification using NIH Image (Automatix, Billerica, MA). Pore diameters were determined by measuring the greatest diameter of the pore (edge to edge) and the length of the pore diameter perpendicular to this line. These two values were averaged for each pore measured, and pore diameter was determined for a minimum of ten pores from each field to derive the mean pore diameter. Interpore distance was measured from center to center of adjacent pores for a minimum of ten pairs of pores in each field. Fiber diameter was determined at three separate locations for each fiber measured, and these values were averaged to determine individual fiber diameter. Diameters were determined for at least ten fibers in each field.

Results

Immunohistochemistry demonstrated the presence of the basement membrane in bladder samples from which the urothelium had been removed (Fig. 1). The basement membranes stained positively for both laminin (Fig. 1) and collagen IV (not shown).

Scanning electron microscopy revealed the surface topography of the urothelial basement membrane to be composed of intertwined fibers and pores of varying sizes (Fig. 2A). Multiple SEM images of three samples from each of the three bladders were reviewed to determine urothelial basement membrane feature heights and pore and fiber diameters. Mean feature height was 178 ± 57 nm. Mean fiber diameter was 52 ± 28 nm, and mean pore diameter was 82 ± 49 nm. The mean interpore distance was 127 ± 54 (Table 1).

Discussion

The appearance and dimensions of the topographic features of the urothelial basement membrane of the rhesus were very similar to those observed for human cornea (Fig. 2B), non-human primate cornea, dog cornea and Matrigel® (Collaborative Research, Bedford, MA), a commercially available basement membrane-like complex employed as a substitute for basement

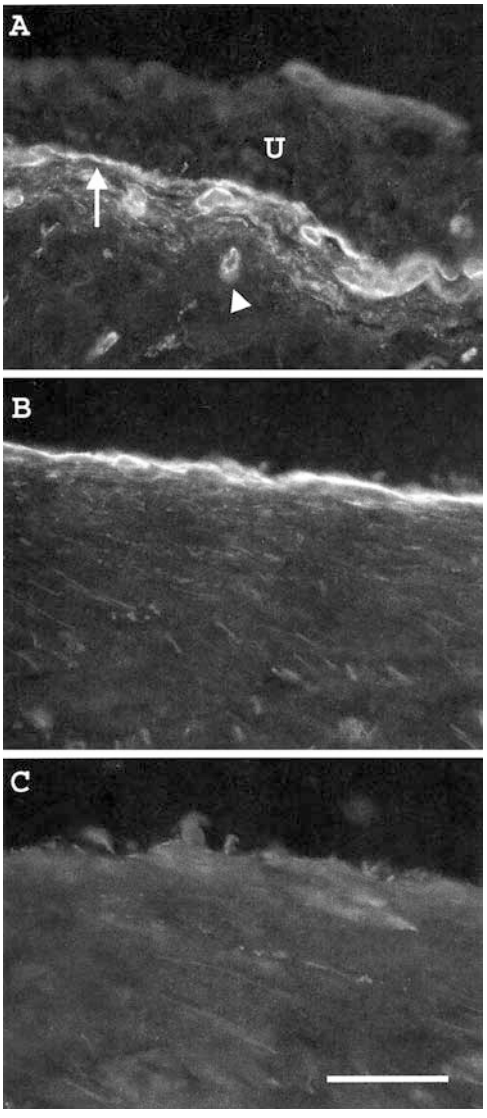

Fig. 1 **A** Immunohistochemical staining for laminin in the bladder wall of the rhesus macaque. The basement membrane (*solid arrow*) found immediately below the urothelium (*U*) stained positively for laminin and collagen IV (not shown). The basement membrane of the blood vessels also stained positively for laminin (*arrowhead*). **B** Removal of the urothelium left the basement membrane intact, and the basement membrane stained positively for both laminin (*arrow*) and collagen IV (not shown). **C** Substitution of normal rabbit IgG for antibody to laminin or collagen IV resulted in an absence of staining of the basement membrane. (Magnification 40×; scale bar = 50 μm)

membrane in cell culture (Fig. 2C, Table 2). In a previous study, we determined the dimensions of topographical features of the human corneal basement membrane and Descemet's membrane using the complimentary techniques of SEM, transmission electron microscopy (TEM), and atomic force microscopy (AFM), and a close correlation was observed among measurements obtained with these techniques [19]. TEM in this previous study was performed on tissues in which the epithelium had not been removed and verified that confounding artifacts had not been introduced into

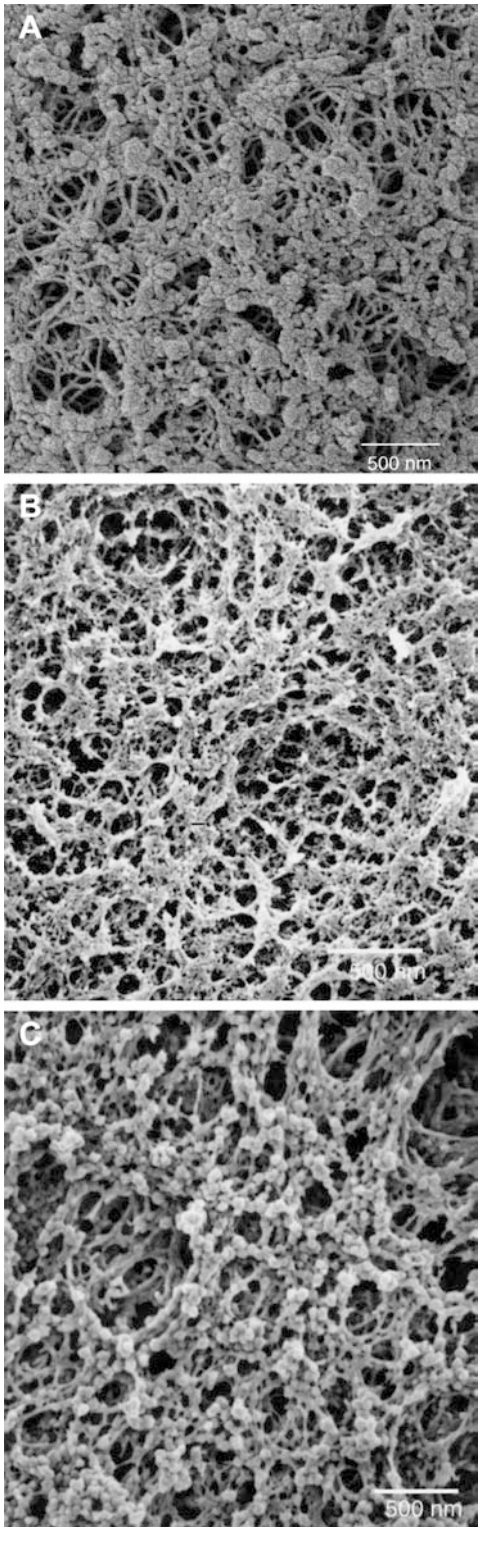

Fig. 2 **A** Scanning electron micrograph of the basement membrane of the urothelium in the rhesus macaque. The surface topography is comprised of intertwining fibers and pores, and appears very similar to the basement membrane of the cornea (**B**), and the surface of Matrigel® (From [19], with permission) (**C**), a commercially available basement membrane-like complex. Collaborative Research, Bedford, MA. (From [20], with permission) (Magnification 30,000×; scale bar = 500 nm

Table 1 Feature dimensions of the rhesus macaque urothelial basement membrane (nm)

	Height	Pore diameter	Fiber diameter	Interpore distance
Mean ± SD	178 ± 57	82 ± 49	52 ± 28	127 ± 54
Median	180	67	49	120
Range	72–287	13–222	13–153	35–349

Table 2 Feature dimensions (mean ± SD) of the corneal basement membranes of the rhesus macaque (macaque), human, and Matrigel®(nm)

Features	Corneal epithelial basement membrane		
	Macaque[a]	Human[b]	Matrigel[a]
Elevations	190 ± 72	182 ± 49	162 ± 52
Pores	71 ± 44	92 ± 34	105 ± 70
Fibers	77 ± 39	46 ± 16	69 ± 35
Interpore distance	87 ± 36	159 ± 72	117 ± 41

[a]Data from [20]
[b]Data from [19]

tissues processed for SEM and AFM. Furthermore, these observations documented that there is a consistent pattern of surface topography of the basement membrane underlying various epithelial surfaces and that the features of basement membrane topography can be accurately determined using SEM alone.

This study did not determine the effects of stretching on the topographical features of the bladder basement membrane. However, we did attempt to stretch each sample to a similar degree. It is possible that stretch could significantly impact the quantitative aspects of basement membrane topography. However, it is interesting to note that quantitative analysis of the bladder basement membrane topography was strikingly similar to those of the basement membrane of a relatively non-elastic tissue (i.e., cornea).

The basement membrane underlying the glomerular and tubular epithelia within the kidney has been studied extensively using SEM and TEM [1, 14, 15, 16, 17]. In general, descriptions of the glomerular and tubular basement membranes are very similar to our observations of the bladder basement membrane. However, estimates of pore size in the glomerular and tubular basement membranes within the kidney have ranged from 5–30 nm and 5–50 nm, respectively [16, 17]. This is significantly smaller than our estimations of pore size in the bladder or corneal basement membranes and may reflect either differences in technique or functional differences of the respective organs. It has been suggested that the basement membrane acts as a sieve to selectively allow the passage of small-diameter molecules, and pore size of the glomerular basement membrane may relate to the physiological need to retain protein within the plasma [12]. The function of pores within the bladder basement membrane is unclear, but these probably serve as channels for passage of small-diameter molecules as well as expanding the potential surface available for interfacing with cells.

There is currently significant interest in bioengineered materials for augmentation or replacement of portions of the urinary tract [25]. Current strategies for development of bioengineered materials for use in the urinary tract typically entail the production of composites consisting of urothelial cells grown on natural or synthetic materials [26, 27]. Composite grafts comprised of urothelium and detrusor muscle seeded onto opposing sides of biodegradable polymers have been used effectively to restore bladder function after partial cystectomy in adult dogs and fetal sheep [28, 29].

While the biocompatibility of urothelial cells with a variety of natural and synthetic substances that might serve as scaffolds for this purpose has been evaluated [30, 31], the influence of surface characteristics on urothelial cell growth and function are unknown. It is clear that the basement membranes perform a variety of functions beyond simply acting as a point of attachment for epithelial cells, but the nature of interaction between epithelial cells and basement membranes, as well as the manner in which the physical properties of basement membranes may influence or direct epithelial cell function, remain unknown. For example, basement membranes play a critical role in corneal wound healing, and the absence of basement membrane delays corneal wound healing for months while a new basement is formed [3, 32]. Cellular responses to changes in the nanoscale topography of underlying surfaces have been evaluated using fabricated materials, and these studies have shown that cellular migration and adhesion is critically affected by the size and orientation of fibers and the depth of grooves between fibers [18]. Cells tend to attach to the tops of ridges, align themselves with the direction of fibers, and migrate along the course of these fibers [33, 34]. Similarly, pore size may critically affect cellular migration and adhesion [35, 36, 37]. The addition of serum to cell culture media facilitates alignment of epithelial cells with nanoscale fibers [18], and it has been suggested that surface characteristics may augment protein localization and presentation to overlying cells [33]. It has been observed that molecular cues that direct cellular organization during embryogenesis are lost in the adult, and it is possible that optimization of the function of bioengineered materials may require simulation of structural and compositional aspects of the embryonic basement membrane [38].

This report provides a detailed description of the nanoscale topographical features of the rhesus macaque urothelial basement membrane. These features are similar to those reported for corneal basement membranes, as well as features found in Matrigel®, a solubilized basement membrane-like matrix obtained from the EHS mouse tumor, which contains components reported for other basement membranes such as collagen, proteoglycans, and laminin. Differences in the concentration of these basement membrane components may explain the subtle differences noted in the appearance and size of

surface features among basement membranes. These finding also indicate that the topographical features of epithelial basement membranes are conserved across species and anatomical locations. We hypothesize that the surface topographical features of basement membranes, in addition to biochemical components of the basement membrane, are important for proper cell signaling to occur and suggest that optimization of the nanoscale surface properties will facilitate development of bioengineered composites for use in urological surgery.

Acknowledgements Funding was from NIH 1RO1 DK57258 (DEB), 1RO1 EY12253 (CJM), and 1RO8 EY00411 (GAA).

References

1. Miner JH (1999) Renal basement membrane components, Kidney Int 56:2016.
2. Miosge N (2001) The ultrastructural composition of basement membranes in vivo. Histol Histopathol 16: 1239
3. Dua HS, Gomes JA, Singh A (1994) Corneal epithelial wound healing. Brit J Ophthal 78: 401
4. Juliano RL, Haskill S (1993) Signal transduction from the extracellular matrix. J Cell Biol 120: 577
5. Mousa SA, Cheresh DA (1997) Recent advances in cell adhesion molecules and extracellular matrix proteins: potential clinical applications. Drug Discov Today 2: 187
6. Bell SE, Mavila A, Salazar R, Bayless KJ, Kanagala S, Maxwell SA, Davis GE (2001) Differential gene expression during capillary morphogenesis in 3D collagen matrices: regulated expression of genes involved in basement membrane matrix assembly, cell cycle progression, cellular differentiation and G-protein signaling. J Cell Sci 114: 2755
7. Li X, Chen Y, Scheele S, Arman E, Haffner-Krausz R, Ekblom P, Lonai P (2001) Fibroblast growth factor signaling and basement membrane assembly are connected during epithelial morphogenesis of the embryoid body. J Cell Biol 153: 811
8. Furuyama A, Iwata M, Hayashi T, Mochitate K (1999) Transforming growth factor-beta1 regulates basement membrane formation by alveolar epithelial cells in vitro. Eur J Cell Biol 78: 867
9. Cosgrove D, Rodgers K, Meehan D, Miller C, Bovard K, Gilroy A, Gardner H, Kotelianski V, Gotwals P, Amatucci A, Kalluri R (2000) Integrin alpha1beta1 and transforming growth factor-beta1 play distinct roles in alport glomerular pathogenesis and serve as dual targets for metabolic therapy. Am J Pathol 157: 1649
10. Ziyadeh FN, Hoffman BB, Han DC, Iglesias-De La Cruz MC, Hong SW, Isono M, Chen S, McGowan TA, Sharma K (2000) Long-term prevention of renal insufficiency, excess matrix gene expression, and glomerular mesangial matrix expansion by treatment with monoclonal antitransforming growth factor-beta antibody in db/db diabetic mice. Proc Natl Acad Sci U S A 97: 8015
11. Inoue S (1994) Basic structure of basement membranes is a fine network of cords, irregular anastomosing strands, Microsc Res Techn 28: 29
12. Merker HJ (1994) Morphology of the basement membrane. Microsc Res Techn 28: 95
13. Ruben GC, Yurchenco PD (1994) High resolution platinum-carbon replication of freeze dried basement membrane. Microsc Res Techn 28: 13
14. Hironaka K, Makino H, Yamsaki Y, Ota Z (1993) Renal basement membranes by ultrahigh resolution scanning electron microscopy. Kidney Int 43: 334
15. Kubosawa H, Kondo Y (1994) Quick-freeze, deep-etch studies of the renal basement membranes. Microsc Res Techn 28: 2
16. Shirato I, Tomino Y, Koide H, Sakai T (1991) Fine structure of the glomerular basement membrane of the rat kidney visualized by high resolution scanning electron microscopy. Cell Tissue Res 266: 1
17. Yamasaki Y, Makino Y, Ota Z (1994) Meshwork structures in bovine glomerular and tubular basement membranes as revealed by ultra-high resolution scanning electron microscopy. Nephron 66: 189
18. Abrams GA, Teixeira AI, Nealey PF, Murphy CJ (2003) The effects of substratum topography on cell behavior. In: Dillow AK, Lowman A (eds) Biomimetic materials and design: interactive biointerfacial strategies, tissue engineering, and drug delivery, Marcel-Dekker, New York, p 91
19. Abrams GA, Schaus SS, Goodman SL, Nealey PF, Murphy CJ (2000) Nanoscale topography of the corneal epithelial basement membrane and Descemet's membrane of the human. Cornea 19: 57
20. Abrams GA, Goodman SL, Nealey PF, Franco M, Murphy CJ (2000) Nanoscale topography of the basement membrane underlying the corneal epithelium of the rhesus macaque. Cell Tiss Res 299: 39
21. Spurr SJ, Gibson IK (1985) Isolation of corneal epithelium with Dispase II or EDTA. Invest Ophthalmol Vis Sci 26: 818
22. Maser MD, Trimble JJ (1977) Rapid chemical dehydration of biological samples for scanning electron microscopy using 2,2-dimethoxypropane. J Histochem Cytochem 25: 247
23. Boyde A (1974) Three-dimensional aspects of SEM images. In: Well OC (ed) Scanning electron microscopy. McGraw-Hill, New York, p 277
24. Goodman SL (1999) Scanning electron microscopy evaluation of biomaterials. In: von Recum AV, Anderson JM (eds) Handbook of biomaterials evaluation: scientific, technical, and clinical testing of implant materials. Taylor and Francis, Philadelphia, p 613
25. Kim BS, Baez CE, Atala A (2000) Biomaterials for tissue engineering. World J Urol 18: 2
26. Atala A (2001) Bladder regeneration by tissue engineering. Br J Urol Int 88: 765
27. Shokeir AA (2002) Bladder regeneration: between the idea and reality. Br J Urol Int 89: 186
28. Oberpenning F, Meng J, Yoo JJ, Atala A (1999) De novo reconstitution of a functional mammalian urinary bladder by tissue engineering. Nat Biotechnol 17: 149
29. Fauza DO, Fishman SJ, Mehegan K, Atala A (1998) Videofetoscopically assisted fetal tissue engineering: bladder augmentation. J Pediatr Surg 33: 7
30. Pariente JL, Kim BS, Atala A (2001) In vitro biocompatibility assessment of naturally derived and synthetic biomaterials using normal human urothelial cells. J Biomed Mater Res 55: 33
31. Pariente JL, Kim BS, Atala A (2002) In vitro biocompatibility evaluation of naturally derived and synthetic biomaterials using normal human bladder smooth muscle cells. J Urol 167: 1867
32. Berman M (1989) The pathogenesis of corneal epithelial defects. Acta Ophthalmol 192 [Suppl]: 55
33. Den Braber ET, Jansen HV, de Boer MJ, Croes HJ, Elwenspoek M, Ginsel LA, Jansen JA (1998) Scanning electron microscopic, transmission electron microscopic, and confocal laser scanning microscopic observation of fibroblasts cultured on microgrooved surfaces of bulk titanium substrata. J Biomed Mater Res 40: 425
34. Van Kooten TG, von Recum AF (1999) Cell adhesion to textured silicone surfaces: the influence of time of adhesion and texture on focal contact and fibronectin fibril formation. Tissue Eng 5: 223
35. Dalton BA, Evans MD, McFarland GA, Steele JG (1999) Modulation of corneal epithelial stratification by polymer surface topography. J Biomed Mater Res 45: 384

36. Fitton JH, Dalton BA, Beumer G, Johnson G, Griesser HJ, Steele JG (1998) Surface topography can interfere with epithelial tissue migration. J Biomed Mater Res 42: 245
37. Steele JG, Johnson G, McLean KM, Beumer GJ, Griesser HJ (2000) Effect of porosity and surface hydrophilicity on migration of epithelial tissue over synthetic polymer. J Biomed Mater Res 50: 475
38. Holmes TC (2002) Novel peptide-based biomaterial scaffolds for tissue engineering. Trends Biotechnol 20: 16